Thermal transfer performance of downhole electric heaters for in-situ pyrolysis in tar-rich coal

Ying TANG [1,2] *, Li XIAO [1], Fan YANG [1], Xiaodan WU [1], Zhan SU [1], Yue ZHANG [1],
Shixin JIANG [1], and Peng YANG [1]

[1] CNOOC Gas & Power Group, Research & Development Center, Beijing, 100028, China
[2] CNOOC Key Laboratory of Liquefied Natural Gas and Low-carbon Technology, Beijing, 100028, China

Abstract. The paper investigates the performance of a large-size helical baffle heater in an in-situ operation using a numerical simulation method. The study reveals that the fluid in the shell retains a spiral flow, and the output flow velocity is higher than in the surrounding area. However, the pitch design is big, resulting in a low-velocity flow zone on the backwind side. At 100 kW and 500 m^3/h, the fluid flow is turbulent. At 50 kW and 200 m^3/h, the fluid remains laminar. As the flow rate rises, the pressure of tar-rich coal formation grows dramatically. The wall temperature exhibits a spiral plunger at the inlet, but the bottom temperature is symmetrically distributed. Under low power and flow, Reynolds number change has a greater impact on the combination of Nusselt and Prandtl numbers. The wellbore experiences higher thermal loads during downhole heating, dramatically increasing the possibility of thermal damage. An increase in the heater shell length improves the total heat transfer performance. Conventional heaters often only heat the bottom formation. Therefore, while optimizing the construction, it is vital to ensure that the weight of the heater itself does not exceed the tensile strength of the cable and consider shifting down the perforation outlet or lowering the outlet.

Keywords: tar-rich coal; in-situ heat injection; downhole heater; thermal performance; well-wall stability.

1. INTRODUCTION

Nonconventional energy sources are gaining prominence, causing a major shift in the global energy environment [1]. Tar-rich coal, a dual-attribute energy resource with coal and hydrocarbon properties, can be transformed into coal tar, pyrolysis gas, and semi-coke using low and medium-temperature pyrolysis, and its development potential is enormous [2, 3]. However, the inefficiency of heat injection in the in-situ mining process has become an important obstacle to the effective production of tar-rich coal [4–6]. As a result, the present study focuses on improving the heat injection mechanism and increasing the efficiency of heat energy consumption [7, 8].

Downhole electric heaters, as a highly efficient energy-saving solution, considerably minimize heat loss during transmission by reducing the distance between the heat source and the reservoir [9]. The Shell E-ICP trial successfully used a Y-type electric heater to heat the formation via heat transfer, proving for the first time the practical use of downhole heaters in unconventional energy study [10]. However, because of the restricted heat transfer area of a single heater and low thermal conductivity in formation, the heating effect is not optimal [11]. To improve the heat transfer performance of downhole electric heaters, researchers began investigating the optimization of the heat transfer structure to increase heat transfer efficiency by causing a change in the fluid flow pattern inside the shell. Traditional bow-shaped

baffle plates may provide transverse flow, but it is accompanied by a flow dead zone, inequality heat transmission, and a shell range pressure decrease [12]. The baffling rod structure may create a longitudinal flow and minimize resistance, but its design is complex and difficult to popularize [13, 14].

In this case, Vukic *et al.* proposed a helical baffle structure that significantly improves heat transfer capacity by forming an approximate plunger flow and enhancing the shell turbulence effect, while effectively avoiding inherent weaknesses of the transverse flow structure [15, 16]. Based on its structural features, the helical baffle is classified into two forms - lap and continuous. Although the lap type has made substantial advances in heat transfer performance, there are still limitations such as insufficient local scouring and the formation of blind zones, particularly at high flow rates, which have a major influence on the heater performance [17]. In contrast to the continuous helical baffle plate, the heat ex-changer structure for electric heating rods provides stable continuous support and shell flow uniformity. The structural parameters have little influence on the stability of the heat transfer performance, which offers a high degree of flexibility and engineering adaptability.

Previous research shows that using downhole heaters in high-temperature conditions can cause casing creep and extra thermal loads, reducing casing strength and stability [18]. According to some research, the axial thermal expansion stress of the casing column is a primary cause of casing breakage during the heavy oil thermal recovery process. Almost 85% of casing damage occurs at the coupling [19], which might be attributed to the coupling material properties, connection method, and insufficient heat exposure [20]. Downhole heating may exacerbate the corro-

*e-mail: tangying@sina.cn

sive effects of fluids in the wellbore, while the high-temperature environment can also cause scaling and deposition [21]. As a result, the integrity of the wellbore is compromised. As thermal mining activities grow, the issue of wellbore integrity failure in geothermal wells owing to thermal stress, corrosion, and clogging becomes more prevalent. To encourage the development of in-situ pyrolysis technology for tar-rich coal resources, this research focuses on one of the most significant technical components of in-situ pyrolysis: the downhole heater. For the investigation of the heat transfer performance and wall stability of the well heater, based on the helical baffle heat transfer structure, the temperature and pressure distribution of the heater, as well as the formation temperature and pressure evolution regulation, were simulated and analyzed using FLUENT. The heat transfer performance under various flow rates and heating powers was comprehensively evaluated, and the influence of the downhole heater on wall stability during the heating process was comprehensively analyzed, with the goal of verifying the heater feasibility and validity. A strong technical support system for the effective development and usage of tar-rich coal will be implemented.

2. MATERIAL AND METHOD

2.1. Test area information

The test area formation is in the Yangjiapo block of Linxing East, which is located in the northern region of Xingxian County, in the Hedong coal field, Shanxi Province. The target coal seam is No. 8 + 9, which has a depth of 1000 meters and a thickness of 10–11 meters. As indicated in Fig. 1. Table 1 shows the special thermophysical properties of tar-rich coal in the test area.
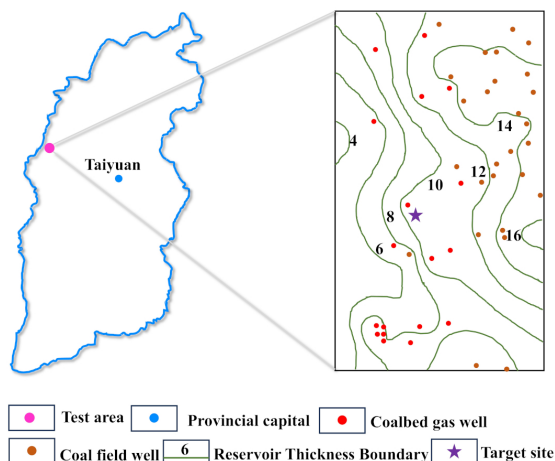

Fig. 1. Test area location

Table 1
Thermophysical parameters of tar-rich coal

Object	Density	Thermal conductivity	Specific heat capacity	Thermal diffusion coefficient
Tar-rich coal	1.48 t/m^3	0.37 W/m·K	1.14 kJ/kgcotK	0.43 W/m·°C

2.2. Physical model

This research proposes a large-size helical baffle heater (LSHB) based on the formation characteristic of the test region. Its primary construction is made up of three parts: a helical baffle, an electric heating rod (heat source), and a shell. The heater is inserted into the well, and gas is pumped into the formation via perforations in the wellbore, which is separated into three layers: upper strata, tar-rich coal formation, and lower strata, as seen in Fig. 2. Table 2 shows the specific structure of LSHB.
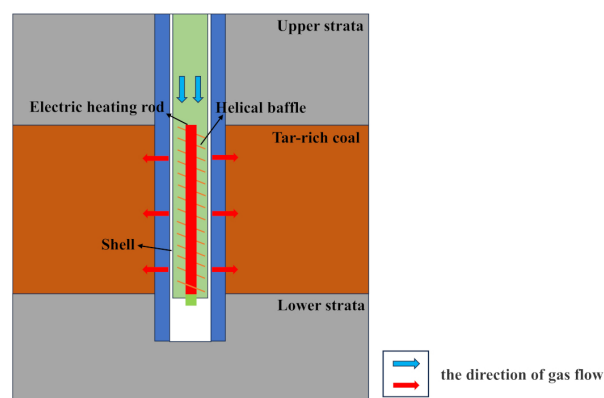

Fig. 2. Schematic diagram of tar-rich coal heating in situ using heater

Table 2
Model structure parameters

Item	Dimension (m)	Item	Dimension (m)
Shell diameter	0.4	Reservoir thickness	10
Wall inside diameter	0.4	Baffle length	10
Wall outside diameter	0.6	Baffle thickness	2×10^{-3}
Upper strata thickness	3	Helical pitch	1.1
Lower strata thickness	3	Heating tube diameter	0.1

2.3. Parameter setting

To appropriately set the simulation starting parameters, the porosity of the tar-rich coal was measured at various temperatures in the test region. In addition, well tests and numerical well tests were conducted on the tar-rich coal reservoir in the test region to determine reservoir pressure and temperature, respectively.

Porosity test samples were acquired using a dry distillation experiment. The heating rate for the dry distillation experiment was 5°C/min, and the temperature was gradually increased from room temperature to 300°C, 400°C, 500°C, 600°C, and 700°C over 30 minutes. Natural cooling was performed for 60 minutes, following which the porosity was determined using the volumetric method. The formation pressure in the test region was then determined using the well test analysis. In addition, the reservoir temperature was determined using numerical well test analysis.

2

Bull. Pol. Acad. Sci. Tech. Sci., vol. 73, no. 3, p. e153839, 2025

Figure 3 depicts the temperature-dependent trend in tar-rich coal porosity. The initial tar-rich coal in the test location had a porosity of less than 10%, which remained stable following pyrolysis at 300°C. This happens given the coal at 300°C only undergoes dewatering, degassing, and carboxylate fracture reaction, and the macroscopic structure of the coal did not change significantly, making the porosity constant. However, the porosity increased significantly to close to 50% when the pyrolysis temperature was up to and higher than 400°C.
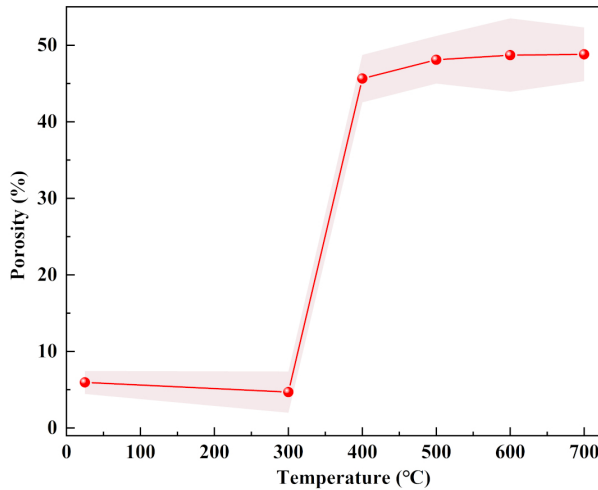

Fig. 3. Tar-rich coal porosity evolution with temperature

Coal reservoir pressure, or the fluid pressure acting on the coal pore and fissure space, also known as pore fluid pressure, has a direct impact on model injection pressure. The experimental findings suggest that the reservoir pressure of coal seam No. 8 + 9 fluctuates between 5.08 to 9.32 MPa, with an average of 7.48 MPa. The pressure gradient ranges from 0.73 to 0.91 MPa/100 m, with an average of 0.82 MPa/100 m. Furthermore, the reservoir temperature has an immediate impact on the model boundary settings. The coal reservoir has a temperature range of 15°C – 31°C, with an average of 22.31°C. The coal seam has a ground temperature gradient of around 2.49°C/100 m, as illustrated in Fig. 4.
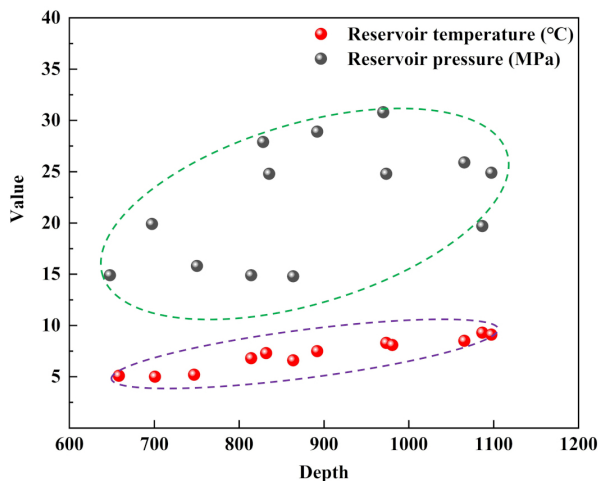

Fig. 4. Reservoir temperature, reservoir pressure vs depth

2.4. Simulated condition

This paper makes the following assumptions for numerical simulations:

- The shell-side fluid was a fully developed turbulent flow in a steady state.
- The fluid in the helical channel is incompressible.
- Heat dissipation on the external wall of the shell cylinder was ignored.
- The heating rod was regarded as a wall with a constant heat flux density.
- The gas inlet temperature was 283 K, and the outlet was a pressure outlet boundary, which follows the constant temperature boundary condition $T_w = 873$ K.
- Tar-rich coal formation was considered a porous medium.

The gas in the heater shell process flows according to the following equations [21]:

The mass conservation equation

$$\frac{\partial \overline{u}_i}{\partial x_i} = 0. \tag{1}$$

The momentum conservation equation

$$\frac{\partial(\rho \overline{u}_i)}{\partial t} + \frac{\partial(\rho \overline{u}_i \overline{u}_j)}{\partial x_j} = -\frac{\partial \overline{p}}{\partial x_i} + \frac{\partial}{\partial X_j}\left(\mu_{\text{eff}} \frac{\partial \overline{u}_i}{\partial x_j} - \rho \overline{u}'_i \cdot \overline{u}'_j\right). \tag{2}$$

The energy conservation equation

$$\frac{\partial}{\partial t}(\rho E) + \frac{\partial}{\partial x_i}\left(u_i(\rho E + p)\right) = \frac{\partial}{\partial x_i}\left(k_{\text{eff}} \frac{\partial T}{\partial x_i}\right) - \sum_{j'} h_{j'} J_{j'} + u_j(\tau_{ij})_{\text{eff}} + S_h, \tag{3}$$

where $E = h - \frac{p}{\rho} + \frac{u_i^2}{2}$; k_{eff} is effective conductivity coefficient $J_{j'}$ is component diffusion flow rate S_h is volumetric heat source.

The universal governing equation for mass, energy, momentum, and RNG k-ε turbulent viscosity is as

$$\text{div}\,(\rho U \Phi) = \text{div}\,(\Gamma_\Phi \text{grad} \Phi) + S_\Phi, \tag{4}$$

where U is the velocity vector; Φ is a universal variable representing; u_i, T, k, ε or another variable; Γ_Φ is a generalized diffusion coefficient, and S_Φ is a generalized source term.

2.5. Energy correction

In this simulation, there is no external energy increase in the energy system, hence the energy absorbed per kilogram of air, Q is defined as [22]

$$Q = (f_{\text{out}} - f_{\text{in}}) + \frac{1}{2}\left(V_{\text{out}}^2 - V_{\text{in}}^2\right) + g\,(Z_{\text{out}} - Z_{\text{in}}) + \Delta W_t, \tag{5}$$

where f is the specific enthalpy of the air; V is the velocity of the shell-side air; g is gravity acceleration; Z is the relative height of the cross-section in the reference system and ΔW_t is the heat loss power per kilogram of air.

Bull. Pol. Acad. Sci. Tech. Sci., vol. 73, no. 3, p. e153839, 2025

3

If we suppose that the air density is constant because the inlet and outlet have the same area, V_{in} is equal to V_{out}. It is assumed that electric energy is completely converted into heat energy during the steady heating of the air.

The heat loss power ΔW per unit time of air is expressed as [23]

$$\Delta W = P_a - (f_{out} - f_{in}) M_s . \tag{6}$$

The effective power P_e is defined as [24]

$$P_e = P_a - \Delta W = (f_{out} - f_{in}) M_s , \tag{7}$$

where P_a is the actual power; M_s is the mass flow rate of the air.

To accurately evaluate the heat transfer performance of the SLSHB, this study utilized the total heat transfer coefficient formula from STHX. The total heat transfer coefficient of the SLSHB was determined by refining the concept of heat transfer temperature difference. The validity of this approach has been confirmed in previous investigations.

The overall heat transfer coefficient K is defined as [24]

$$K = \frac{P_e}{A \Delta t_m} . \tag{8}$$

The logarithmic heat transfer temperature difference Δt_m is defined as

$$\Delta t_m = \frac{\Delta t_{max} - \Delta t_{min}}{\ln \left(\dfrac{\Delta t_{max}}{\Delta t_{min}} \right)} , \tag{9}$$

where A is the total heat transfer area of the heating rod; Δt_{max} is the temperature difference between the temperature on the heating rod surface and the temperature at the top-most fluid outlet and Δt_{min} is the temperature difference between the heating rod surface and the temperature at the bottom fluid outlet. The surface temperature of the heating rod was obtained by linear interpolation of the surface temperature measured at the fully expanded section of the heating rod.

The Reynolds number R_e of the SLSHB is defined as [25]

$$R_e = \frac{d_e U_s \rho}{\mu} , \tag{10}$$

where d_e is the hydraulic diameter of the shell side; U_s is the velocity of the shell side; ρ is the characteristic density of the shell-side air and μ is the characteristic viscosity of the shell-side air.

The convective heat transfer coefficient h of the heating rod surface is defined as [26]

$$h = \frac{\lambda N_u}{d_e} , \tag{11}$$

where λ is the thermal conductivity of the heating rod material.

The shell-side Nusselt number N_u is defined as [27]

$$N_u = C R_e^m P_r^{\frac{1}{3}} . \tag{12}$$

The shell-side Prandtl number P_r is defined as [27]

$$P_r = \frac{C_p \mu}{\lambda} . \tag{13}$$

The thermal resistance of an SLSHB is defined as [28]

$$\frac{1}{K} = \frac{1}{h} + R_f . \tag{14}$$

Because the SLSHB is new, the fouling resistance R_f is not considered, and the following equation can be obtained

$$K = h. \tag{15}$$

2.6. Test scheme

In this experiment, the heater outlet was set to function in a free-flow state, and a constant heating power scheme was used to thoroughly evaluate heater performance. The inlet and output gas temperatures, pressures, and surface temperature of the heater rod were all measured. Furthermore, the shell-side Reynolds number and total heat transfer coefficient were investigated at various heating powers and gas flow rates. Cross-over tests were conducted to determine heater performance at two distinct gas flow rates and heating power levels.

3. RESULTS AND ANALYSIS

3.1. Shell flow characterization

Figures 5 and 6 show the distribution of the flow rate and the trajectory of the fluid in the heater during in-situ heating. Inside the LSHB shell, the fluid has a consistent spiral flow pattern, and the flow rate drops gradually and consistently along the
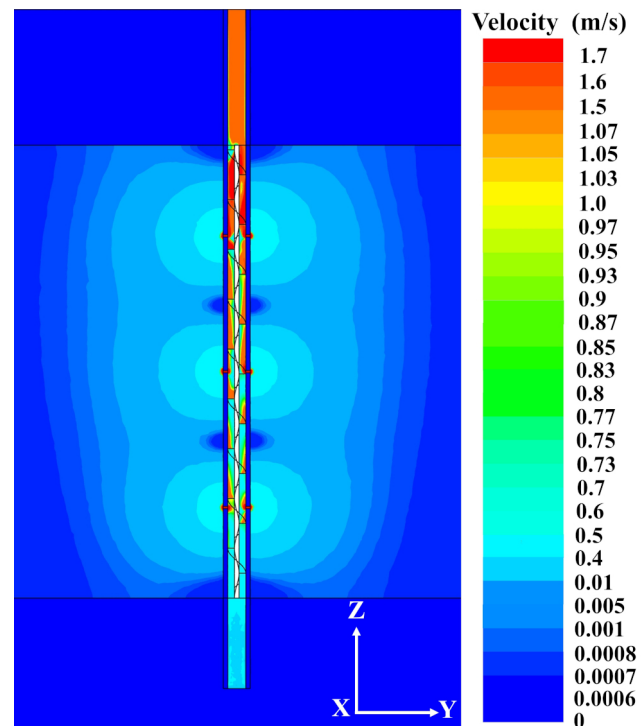
Fig. 5. Characterization of the fluid in the shell (500 m³/h)

4

Bull. Pol. Acad. Sci. Tech. Sci., vol. 73, no. 3, p. e153839, 2025

direction of flow. This unique flow feature guarantees that the fluid flows uniformly and continuously across the surface of the heater rod, eliminating excessive heat rod concentration, which significantly improves the LSHB heater stability and dependability in difficult downhole working conditions. This function is especially significant for LSHB heaters with lengths more than 10 meters since it guarantees that the heater maintains an effective and consistent heating effect along its length. While the fluid flow rate reduces as the shell is expanded, the flow rate increases significantly near the fluid outlet, which is where the perforations are located. The fluid channel is abruptly constricted at the position of the perforations, causing the fluid to flow quicker as it exits the heater. The higher flow rate improves heat exchange efficiency between the fluid and the heater rod to some extent, hence boosts the overall effectiveness of the heater.
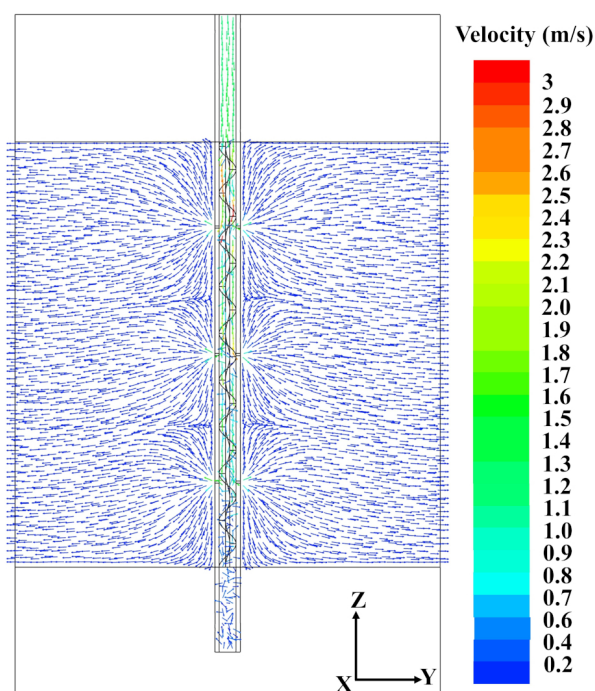

Fig. 6. 6. Flow field trajectory (500 m³/h)

During the extensive inspection, we also discovered a distinct zone of low-velocity fluid flow on the backwind side of the baffle. This problem is the result of an extremely large pitch design, which inhibits fluid movement in this location. The presence of this low velocity zone cannot be overlooked, as it may cause the fluid to not touch and cool the heater rod uniformly, resulting in localized overheating of the central rod, posing a real and possible risk to heater lifetime. As a result, while optimizing the future structure design, we must consider the heater pitch size. By adjusting the pitch appropriately, we can guarantee that the fluid throughout the heating process maintains a consistent and efficient flow state, which not only extends the utilizable life of the heater but also considerably improves its overall performance [2].

Figure 7 demonstrates that the Reynolds number gradually decreases as temperature increases. This is because increasing the
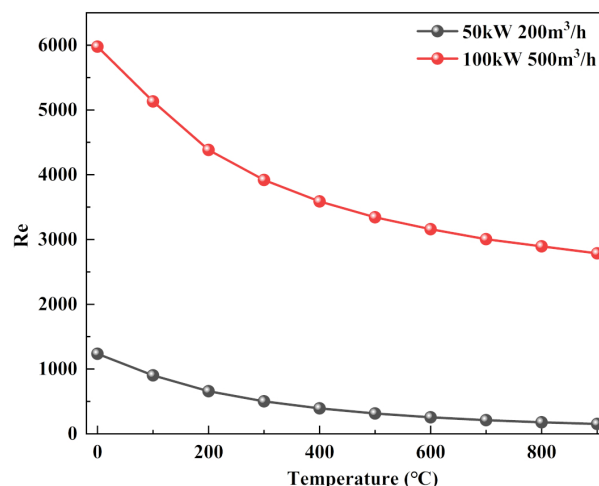

Fig. 7. Re number versus temperature

temperature causes a rise in fluid viscosity, which increases flow resistance and reduces the Reynolds number. In addition, the heater top-down perforation design contributes to the Reynolds number decline. At 50 kW, the decline in Reynolds number is very gentle, but at 100 kW, it becomes more significant. This is because more heating power causes the gas to heat up faster over the same flow distance, resulting in a more dramatic change in the fluid flow condition. In 100 kW, 500 m³/h, the fluid flow pattern presents a turbulent pattern, which under the heat transfer effect is relatively better. As the flow distance increases, the flow pattern shifts from turbulence to laminar flow, which means that the temperature at the bottom of the heater is the highest, but the heater's heat transfer efficiency may not be the best. In 50 kW, 200 m³/h, the fluid flow maintains a laminar flow pattern, which is more stable but has lower heat transfer efficiency compared to the former.

3.2. Pressure characterization

Figure 8 clearly shows that there is no significant loss of pressure in the shell when the number of perforations in the wellbore rises. This phenomenon is mostly linked to the original experimental parameter and the meticulous design of the heater. Throughout the studies, the flow rate of the injected fluid was kept substantially greater than the flow rate of the fluid output, ensuring that there was always enough gas within the heater. This design not only helps to maintain a consistent flow of gas inside the heater, but it also guarantees that the heating process runs constantly and effectively. The bigger volume implies that the heater can manage more gas, which improves heating efficiency and capacity. In reality, this implies that the heater can heat more gas to the desired temperature in less time, giving significant support for in-situ heating.

In addition, a larger injection flow effectively compensates for any pressure loss that may occur during the use of the heater. Even if some pressure loss occurs, it can be quickly replenished by continuous injection of additional gas, thus maintaining a stable pressure inside the heater. This design not only improves the reliability and stability of the heater but also ensures smooth in-situ heating.
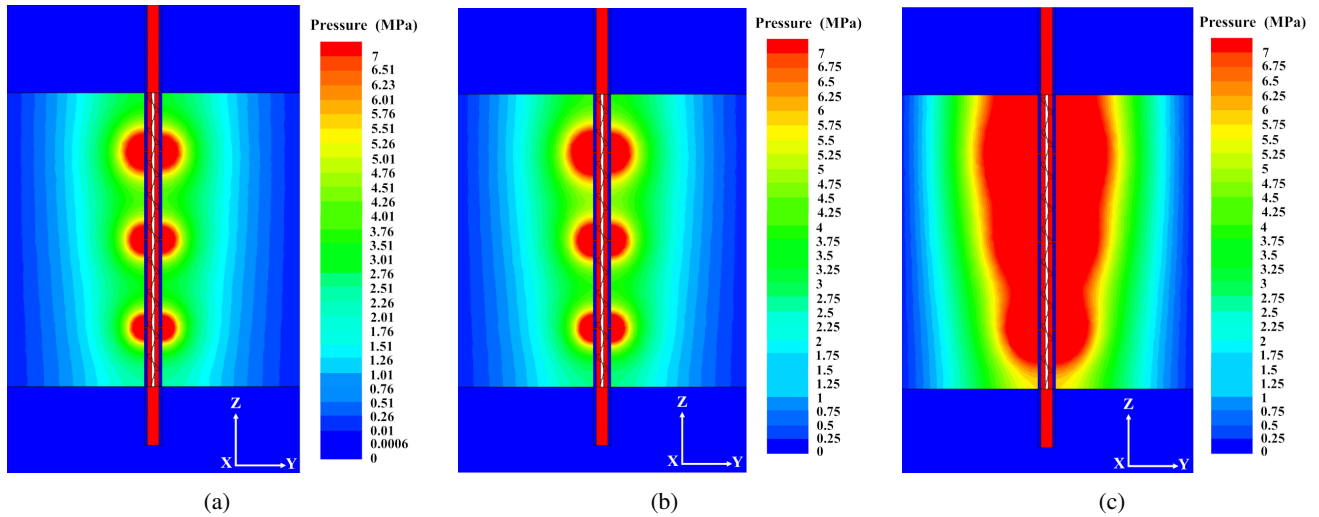
Fig. 8. Pressure distribution under in-situ operation of the heater: (a) 50 kW, 200 m^3/h; (b) 100 kW, 200 m^3/h; (c) 100 kW, 500 m^3/h

Figures 8a and 8c indicate that the pressure in the tar-rich coal formation increases significantly as the injection flow increases. This alteration is of critical relevance to in-situ heating. The increased pressure in the formation indicates that the convective heat transfer of gas in the formation will be greatly improved. Convective heat transfer is one of the primary ways of heat transmission in in-situ heating. It ensures uniform heating for the whole formation by transferring heat from the heater to the gas in the formation, which then passes the heat to the surrounding coal body.

When formation pressure rises, gas flows through the formation at a higher pace, making convective heat transfer more effective. The quicker the gas flows, the more heat it can take away and transfer to a longer distance, widening the heating range and enhancing heating efficiency. This gain effect is extremely beneficial to the development of in-situ heating, as it may minimize the heating time and energy consumption and

enhance oil recovery. Aside from the gain impact of convective heat transfer, a rise in formation pressure improves other conditions in in-situ heating. According to previous studies, formation pressure can enhance formation permeability, making it simpler for gases to move and disperse inside the formation. Simultaneously, it can increase the thermal conductivity of tar-rich coal, making heat transmission and diffusion simpler. All of these enhancements contribute to the overall effectiveness of in-situ heating and provide more robust support for the efficient use of tar-rich coal resources [23, 29].

3.3. Temperature characterization

Figure 9 demonstrates that as the length of the heater shell grows, so does the shell temperature, and the formation temperature follows suit. As the fluid goes via various perforated outlets, the flow velocity and scouring of the heater rods reduce, resulting in a steady increase in temperature at the heater bottom. Further-
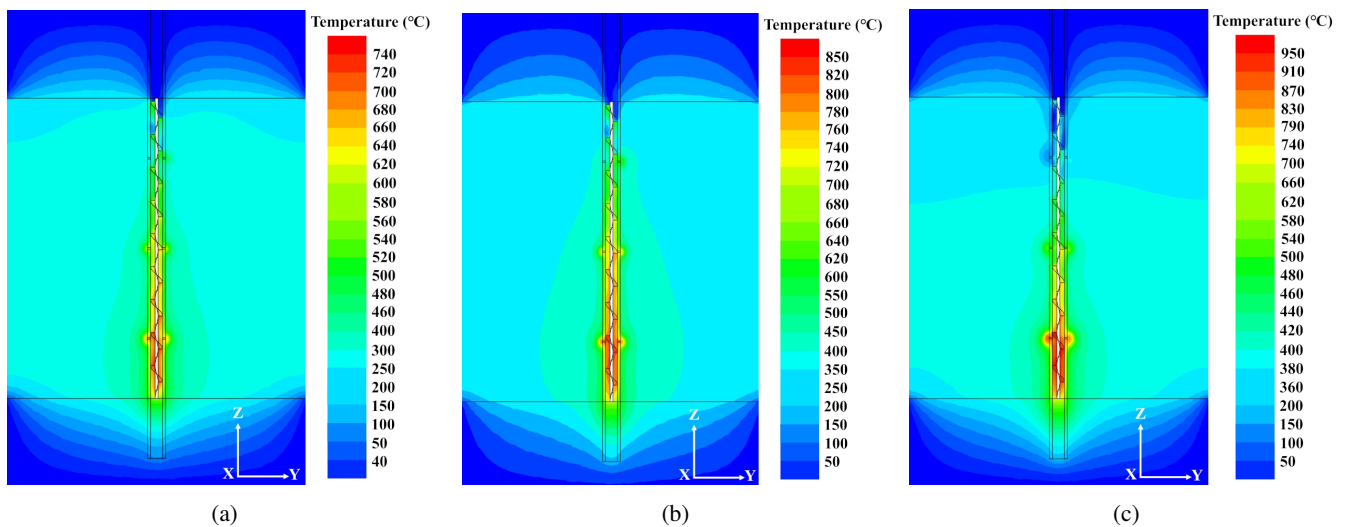

Fig. 9. Temperature distribution under in-situ operation of the heater: (a) 50 kW, 200 m^3/h; (b) 100 kW, 200 m^3/h; (c) 100 kW, 500 m^3/h

more, increased fluid viscosity exacerbates the situation. Other helical baffle heaters have the same phenomena of rising temperature at the bottom as the heater shell climbs. The shell-side perforation does not affect this phenomenon, which is inherent in helical baffle plates.

When Figs. 9a and 9b are compared, the temperature at the outlet of the lowest perforation gradually rises and exceeds that of the surrounding formation, and this warming trend gradually spreads to the location of the middle perforation outlet, which is primarily caused by increasing the heating power of the center heating rod. Figure 9c shows this warming process more clearly. Observing the overall temperature distribution reveals that this sort of heater can greatly enhance the temperature of the tar-rich coal formation, particularly the tar-rich coal formation in the lower center. During the heating phase, the tar-rich coal formation warms the surrounding formation via conduction.

3.4. Characterization of wall temperatures in heat injection well

Figure 10 depicts several interesting and relevant elements in the wall temperature distribution under various conditions. It is evident that the wall temperature steadily increases with the depth of the heat injection, which is quite similar to the heater temperature distribution pattern. This likeness is not a coincidence, because the heat created by the heater as a heat source is progressively transmitted to the wall by heat conduction and convective heat transfer, increasing wall temperature.
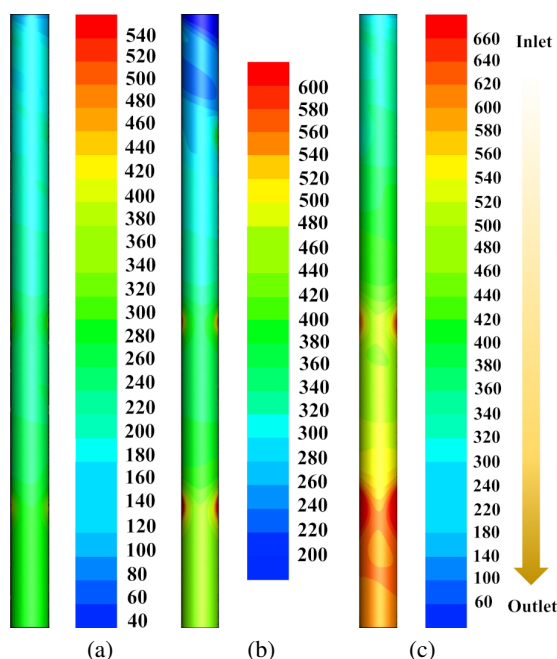

Fig. 10. Wall temperature distribution in heat injection well

Closer to the inlet, the wall temperature resembles a spiral plunger flow. This is because the gas at the inlet has just entered the heater and has not yet been exposed to the heating rod's high-temperature stress. Hence, its flow pattern is symbolized by a spiral plunger flow. This flow pattern enhances heat exchange

between the gas and the heater rod, causing the wall temperature at the inlet to rise fast. As the fluid flows and the heating proceeds, the temperature at the perforation outlet may rise above that of the surrounding wall, as seen in Figs. 10b and 10c. This phenomenon occurs because the flow velocity at the perforation outlet is higher, resulting in a greater convective heat transfer impact. When the fluid flows out of the heater at a faster rate, it removes a substantial quantity of heat and strongly exchanges heat with the surrounding wall, resulting in a comparatively high wall temperature at the perforation outlet.

As the heater shell length and the number of perforation outlets grow, the convective heat transfer impact of gas rapidly diminishes. This is because increasing the length of the shell and the number of perforated outlets creates a more complicated and convoluted flow path for the gas in the heater, causing the flow velocity to slow down and limiting the effectiveness of convection heat transfer. In addition, as the heating progresses, the temperature difference between the heater and the gas narrows, making convective heat transfer less effective. Because the gas flow rate at the bottom of the heater is sluggish, the wall temperature is often conveyed by heat conduction. In the heat transfer process, the heating rod heats the gas in the shell, which subsequently transmits heat to the well wall. Furthermore, because the heating rod is positioned in the middle of the heat injection well, the temperature distribution at the wall bottom will be symmetrical, with the heat injection well serving as the symmetry axis.

This temperature distribution feature is critical for the in-situ exploitation of tar-rich coal reserves. A reasonable use of this temperature distribution function can considerably increase heat transfer efficiency and lifetime. For example, reduce the pitch, increase the shell length, and reasonably arrange the location and number of perforation outlets, optimize the flow path and flow time of the fluid in the heater, so that there is fuller interaction between the fluid and the heating rod for heat exchange, and there is improvement in the flow rate of gas and convective heat transfer effect. The above optimization approaches can greatly increase the heat transfer efficiency and lifespan, resulting in a more efficient and dependable heating solution for in-situ mining of tar-rich coal reserves.

Wellbore materials (such as steel casing) can produce thermal strains during downhole heating as a result of thermal expansion and contraction. Although this stress may not be substantial in the short run, long-term consequences affect the material microstructure, increasing the chance of fatigue, cracking, and even fracture. When the heating temperature exceeds the material endurance limit, the mechanical properties of the material are significantly reduced (e.g., lower strength and weaker toughness), making the wellbore more susceptible to deformation or damage when subjected to external pressure or internal fluid impact. Furthermore, the uneven wall temperature distribution induced by downhole heating is a concern that should not be overlooked. The temperature of the wellbore wall may fluctuate depending on the position of the heating source, the heating power, and the thermal conductivity in the formation, resulting in a temperature gradient. This temperature gradient not only concentrates thermal stresses in the wellbore material, but it can also cause

Bull. Pol. Acad. Sci. Tech. Sci., vol. 73, no. 3, p. e153839, 2025

7

the wellbore to deform axially or radially. In particular, in areas with large temperature gradients, such as near a heating source or where the thermal conductivity of the formation changes abruptly, the concentration of thermal stresses may exceed the ultimate strength of the material, causing localized damage to the wellbore. Localized elevated temperatures may develop in some portions of the wellbore, producing thermal damage to the material (e.g., carbonization, melting), which poses a major danger to the structural integrity of the wellbore. As a result, selecting appropriate high-temperature-resistant materials and a fair range of heating temperatures is critical to assuring the wellbore structural safety.

In conclusion, despite 50 kW and 200 m^3/h, the wall temperature at the inlet remains over 160°C, which is detrimental to the well-wall stability. The range of thermal stress impact grows in proportion to the wall temperature gradient. According to field experience [30], the thermal expansion impact of the well wall is insignificant when the wall temperature is less than 50°C. As a result, given the parameters of this simulation, the wall temperature effect ranges between 20 and 40 meters.

3.5. Thermal characterization

According to equations (8)–(15), the relationship between the overall heat transfer coefficient and the shell-side flow field can be expressed as [30]

$$\ln\left(N_u P_r^{-\frac{1}{3}}\right) = D\ln(R_e) + \ln(C). \tag{16}$$

The following equation can be obtained by the linear regression of (16)

$$Y = DX + b, \tag{17}$$

where $X = \ln(R_e)$, $Y = \ln\left(N_u P_r^{-\frac{1}{3}}\right)$, and $b = \ln(C)$. The regression parameters are listed in Table 3.

Table 3
Regression parameters

Test	C	m	K (W·m^{-2}·K^{-1})
50 kW, 200 m^3/h			0.1764
100 kW, 200 m^3/h	0.175	0.9213	0.3704
100 kW, 500 m^3/h			0.1946

The linear regression equation properly depicts the fundamental relationship between the Nusselt number, Prandtl number, and Reynolds number. Figure 11 shows that the fitting of both regression curves is 0.96 or higher, proving the regression equation dependability and correctness.

The regression curve shows a slope of around 0.7645 for 100 kW power and 500 m^3/h flow rate, and 0.8844 for 50 kW power and 200 m^3/h flow rate. This disparity suggests that changing the Reynolds number has a greater impact on the combination of Nusselt number and Prandtl number under low power and flow conditions, in other words, when the fluid is at
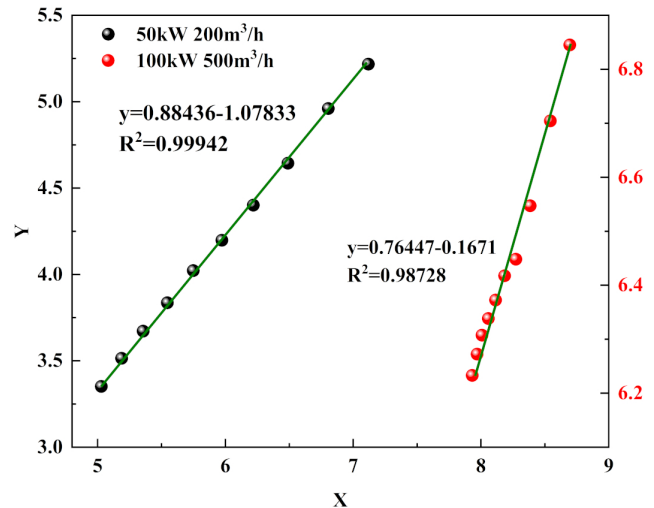

Fig. 11. Heat transfer correlation

low power and low flow, it transitions from laminar to turbulent flow more quickly, which contributes to increased heat transfer efficiency. In the 50 kW, 200 m^3/h, the intercept is 1.0783, whereas the 100 kW, 500 m^3/h has an intercept of 0.1671. This disparity shows a major variance in the heat exchanger efficiency of the heater under various base conditions. Specifically, for low Reynolds numbers, high power, and flow rate conditions result in a slight decline in the heat transfer performance. This discovery is a useful guideline for adjusting heater operating settings and increasing heat transfer efficiency.

The gas temperature rises as the gas flow channel within the heater shell expands. Figure 12 depicts the temperature-dependent trend of the convective heat transfer coefficient, which reflects the complexity of fluid movement and heat transmission within the heater. The convective heat transfer coefficient declines with shell length at 50 kW and 200 m^3/h but steadily increases at 100 kW and 500 m^3/h. The low gas injection flow rate of 200 m^3/h at 50 kW prevents effective convective heat transfer between the gas and heating rod. However, convection is more effective at 100 kW and 500 m^3/h.
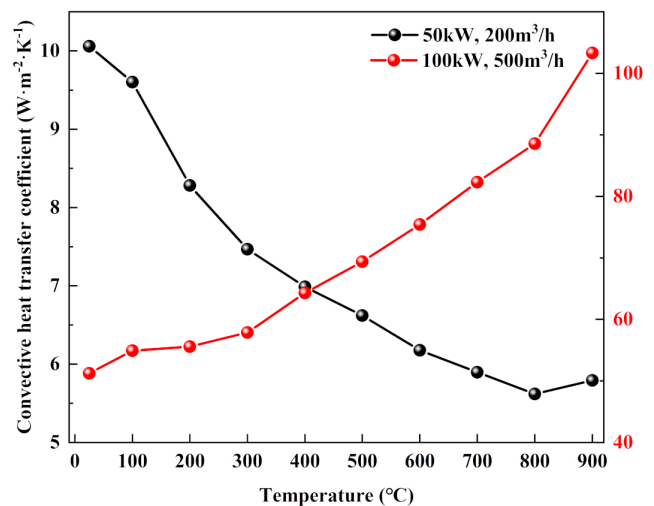

Fig. 12. Convective heat transfer coefficient vs temperature

8

Bull. Pol. Acad. Sci. Tech. Sci., vol. 73, no. 3, p. e153839, 2025

As the gas moves along the heater shell, its flow condition and time, which has a substantial impact on heat transmission. On the one hand, the gas in the flow continues to absorb heat, and the temperature steadily rises, causing changes in the physical properties of gas (such as density and viscosity), influencing the size of the Reynolds number. Figure 7 demonstrates that the Reynolds number gradually decreases as the gas temperature increases. As the Reynolds number decreases, the fluid flow stabilizes and the turbulence degree decreases, affecting the efficiency of convective heat transmission to some extent. The heater, on the other hand, is constructed with several perforated outlets in the heater shell, which causes the gas to continually diverge during the flow, thus reducing the flow rate. The slower flow rate increases gas residence time inside the heater and the contact time with the heating rods, providing more possibilities for heat exchange. The increase in heat transfer coefficient is compounded by the greater heating rate and, as a result, the rate of gas warming in the shell, particularly at 100 kW.

3.6. Comprehensive assessment

The crucial parameters for evaluating heater performance are $h/\Delta P$ and $h/\Delta P^{\frac{1}{3}}$. This option is meant to more accurately portray heater balanced connection between heat transfer efficiency and energy usage [29].

Figure 13 depicts the tight link between the heater shell length and total heat transfer performance. The temperature at the bottom of the heater rises as the shell length grows, which directly affects the gas viscosity during flow. As viscosity rises, the internal friction of the gas flow increases, and the flow rate decreases, lengthening gas residence time in the heater and offering a greater chance for heat transfer between the gas and the heating rod. As a result, the heat transfer coefficient increases, improving the total heat transfer performance of the heater. This phenomenon is especially evident in simulation experiments with varying heating powers, where the improvement in the heat transfer coefficient is more pronounced under the high-power condition because more heat is generated by the heating rod, the temperature of the gas rises faster, and the viscosity change is greater.
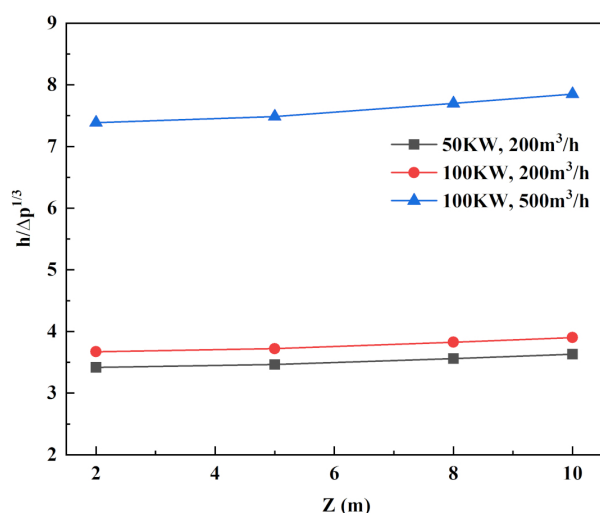
However, when focusing on great thermal efficiency, we must not overlook the energy consumed during heater operation. In the same heat transfer structure, raising the injection flow rate can minimize pressure loss in the shell, which looks to benefit the overall heat transfer performance of the heater. In reality, this increase is ineffective, particularly at low power levels (for example, 50 kW). This is because, while reduced pressure losses reduce energy consumption, higher injection flow requires more gas to be supplied by surface equipment, increasing the cost of mining and exploiting unconventional energy sources. With the rising cost of energy extraction, this additional input might be a significant obstacle to the improvement of the overall heater performance.

As a result, while optimizing heater design and enhancing heat transfer efficiency, we must consider a wide range of elements. On the one hand, it is required to increase the heat transfer coefficient by adjusting heater structural characteristics (e.g., shell length, heating rod arrangement, etc.) so that the heater can fully use thermal energy while working effectively. On the other hand, it is vital to monitor energy usage and lower heater running costs through proper flow control and pressure loss management. Furthermore, to optimize the overall performance of the heater, the long-term stability of its operation, maintenance costs, and environmental friendliness must all be considered.

Finally, full performance evaluation of heaters is a complicated and diverse task. When picking assessment indexes, we should consider the real working environment and application needs of the heater. When optimizing the design, heat transfer efficiency, energy consumption, cost, and environmental impact should all be addressed to obtain the optimal balance of the heater overall performance [31].

4. CONCLUSIONS

This work investigates the heat transfer performance of a large-size helical baffle heater aiming to improve a critical heating step for in-situ pyrolysis of tar-rich coal resources. Fluent numerical simulation was used to thoroughly analyze the heater temperature and pressure distribution, as well as the wall temperature, in the heat injection well under in-situ conditions, while orthogonal simulation was used to investigate heat transfer and overall performance under various injection flow rates and heating powers. The study initially proved the heater in-situ viability and provided a foundation for its further structural optimization.

It can be concluded that the fluid in the shell program flows in a spiral pattern with a steadily declining flow velocity, the exit flow velocity is much greater than the surrounding area, and a low-velocity flow zone exists on the backwind side of the baffle plate. The increased temperature causes a reduction in the Reynolds number, which is worsened by the sidewall perforations outflow. At high power and flow rates, the fluid flow becomes turbulent, but at low power and flow rates, the fluid flow remains laminar. The increased openness of the sidewall perforations causes no substantial pressure loss, and the high injection flow rate compensates for the pressure loss, increases formation pressure, and promotes gas convective heat transfer.

Fig. 13. Comprehensive evaluation vs. heater route

Bull. Pol. Acad. Sci. Tech. Sci., vol. 73, no. 3, p. e153839, 2025

9

- The shell temperature rises with length, and the fluid outlet temperature at the bottom is the greatest, spreading toward the center, while the heating process is accompanied by heat transmission to the surrounding formation. The temperature of the well wall rises with the depth of the heat injection well, indicating spiral plunger flow characteristics at the input; the temperature at the outlet may be greater than the wall; and the temperature distribution at the bottom is symmetrical.
- At low power and high flow rate, changing the Reynolds number has a major influence on heat transfer efficiency, as the fluid transitions from laminar to turbulent flow more quickly, hence increasing heat transfer. At low Reynolds numbers, the heat transfer performance of the heater is slightly poorer at high power and flow rates.
- Heater shell length rises, as does bottom temperature, gas viscosity, flow rate, heating duration, and heat transfer coefficient, all of which enhance total heat transfer performance. In the same heat transfer structure, raising the injection flow rate has an insignificant effect on lowering pressure loss and enhancing total heat transfer performance, particularly under low power.
- Conventional heaters have a restricted heating scope; this heater may increase the heating scope, enhance the convection heat transfer effect, and have a smaller diameter, allowing for a wider range of applications. The pitch is too large, resulting in insufficient limitations on the gas flow pattern, and the position and number of perforations on the side wall significantly affect the heating range. Structural optimization should consider the weight of the heater concerning cable tensile strength, and it is advised that perforations be moved down or reduced in number.

ACKNOWLEDGEMENTS

REFERENCES

[1] M. Li, X. Cheng, J. Hao, Z. Lu, and J. Wei, "Experimental and numerical investigation on the heat and mass transfer performance of tar rich coal in-situ pyrolysis," *Int. J. Heat Fluid Flow.*, vol. 107, p. 109412, Jul. 2024, doi: 10.1016/j.ijheatfluidflow.2024.109412.

[2] Z. Wang *et al.*, "Study on pore structure and fractal characteristics of tar-rich coal during pyrolysis by mercury intrusion porosimetry (MIP)," *Geofluids*, vol. 2022, p. 2067228, Oct. 2022, doi: 10.1155/2022/2067228.

[3] D. Fu *et al.*, "Thermodynamic analysis on in-situ underground pyrolysis of tar-rich coal: Secondary reactions," *ACS Omega*, vol. 8, no. 14, pp. 12805–12819, Apr. 11 2023, doi: 10.1021/acsomega.2c08033.

[4] L. Ma *et al.*, "Investigation of pyrolysis and mild oxidation characteristics of tar-rich coal via thermogravimetric experiments," *ACS Omega*, vol. 7, no. 29, pp. 25613–25624, Jul 26 2022, doi: 10.1021/acsomega.2c02786.

[5] Q. Shi *et al.*, "Experimental study on the tar and gas distribution during tar-rich coal pyrolysis with stress loading," *Fuel*, vol. 376, p. 132727, Nov. 2024, doi: 10.1016/j.fuel.2024.132727.

[6] F. Yang *et al.*, "Thermodynamic analysis of in-situ underground pyrolysis of tar-rich coal: Primary reactions," *ACS Omega*, vol. 8, no. 21, pp. 18915–18929, May 2023, doi: 10.1021/acsomega.3c01321.

[7] Y. Hu, Y. Bao, J. Meng, D. Li, X. Yuan, and Z. Dong, "Biomethane production efficiency and degradation mechanism of tar-rich coal in anaerobic digestion," *Fuel*, vol. 375, p. 132560, Nov. 2024, doi: 10.1016/j.fuel.2024.132560.

[8] W. Guo *et al.*, "Effects of packer locations on downhole electric heater performance: experimental test and economic analysis," *Energies*, vol. 13, no. 2, p. 377, Jan. 2020, doi: 10.3390/en13020377.

[9] Z. Kang, Y. Zhao, and D. Yang, "Review of oil shale in-situ conversion technology," *Appl. Energy*, vol. 269, p. 115121, Jul. 2020, doi: 10.1016/j.apenergy.2020.115121.

[10] Y. Chen, H. Zeng, J. Wang, H. Chen, and J. Zhu, "Heat transfer performance of a downhole electric tubular resistive heater," *Appl. Sci.*, vol. 12, no. 19, p. 9508, Oct. 2022, doi: 10.3390/app12199508.

[11] F. Fei, Y. Chen, J. Wu, J. Su, and H. Gu, "Numerical comparison of orifice, ladder helical or segmental baffle half-cylindrical heat exchangers," *Heat Transfer Eng.*, vol. 45, pp. 1974–1988, 2023, doi: 10.1080/01457632.2023.2289231.

[12] D.V. Lesnoy and S.K. Churakova, "Segmental baffles as a means of improving the heat transfer efficiency of air coolers," *Chem. Pet. Eng.*, vol. 57, no. 1–2, pp. 106–112, May 2021, doi: 10.1007/s10556-021-00902-3.

[13] J. Zhang, S. Guo, Z. Li, J. Wang, Y. He, and W. Tao, "Experimental performance comparison of shell-and-tube oil coolers with overlapped helical baffles and segmental baffles," *Appl. Therm. Eng.*, vol. 58, no. 12, pp. 336–343, Sep. 2013, doi: 10.1016/j.applthermaleng.2013.04.009.

[14] M.F. Nia, H. Farzad, A.B. Ansari, M. Ghodrat, S.A.G. Nassab, and M. Behnia, "Performance improvement of a tubular heat exchanger by tube arrangement optimization using simulated annealing algorithm and blocked-off method," *Therm. Sci. Eng. Prog.*, vol. 40, p. 101793, May 2023, doi: 10.1016/j.tSep.2023.101793.

[15] M.V. Vukic, M.A. Tomic, P.M. Zivkovic, and G.S. Ilic, "Effect of segmental baffles on the shell-and-tube heat exchanger effectiveness," *Hem. Ind.*, vol. 68, no. 2, pp. 171–177, Mar.-Apr. 2014, doi: 10.2298/hemind130127041v.

[16] E.M. S. El-Said and M.M. Abou Al-Sood, "Shell and tube heat exchanger with new segmental baffles configurations: A comparative experimental investigation," *Appl. Therm. Eng.*, vol. 150, pp. 803–810, Mar. 2019, doi: 10.1016/j.applthermaleng.2019.01.039.

[17] X. Gu, N. Li, C. Chen, Q. Zhang, G. Wang, and Y. Wang, "Analysis of fluid retention zones in heat exchangers with segmental baffle and helical baffle," *Int. J. Chem. React. Eng.*, vol. 20, no. 7, pp. 681–696, Jul. 2022, doi: 10.1515/ijcre-2021-0230.

[18] Z. Wang, P. Wang, D. Zeng, T. Shi, and W. Deng, "A study on the influential factors of stress corrosion cracking in C110 casing pipe," *Materials*, vol. 15, no. 3, p. 801, Feb. 2022, doi: 10.3390/ma15030801.

10

Bull. Pol. Acad. Sci. Tech. Sci., vol. 73, no. 3, p. e153839, 2025

[19] L. Cai, G. Xu, M.A. Polak, and M. Knight, "Horizontal directional drilling pulling forces prediction methods – A critical review," *Tunnelling and Underground Space Technology*, vol. 69, pp. 85–93, Oct. 2017, doi: 10.1016/j.tust.2017.05.026.

[20] W. Guo *et al.*, "Experimental investigation on performance of downhole electric heaters with continuous helical baffles used in oil shale in-situ pyrolysis," *Appl. Therm. Eng.*, vol. 147, pp. 1024–1035, Jan. 2019, doi: 10.1016/j.applthermaleng.2018.11.013.

[21] C. Dong, Y. Chen, and J. Wu, "Flow and heat transfer performances of helical baffle heat exchangers with different baffle configurations," *Appl. Therm. Eng.*, vol. 80, pp. 328–338, Apr. 2015, doi: 10.1016/j.applthermaleng.2015.01.070.

[22] J. Shui, D. Wenjing, W. Peng, and C. Lin, "Numerical investigation on double shell-pass shell-and-tube heat exchanger with continuous helical baffles," *J. Thermodyn.*, vol. 2011, pp. 651–654, 2011.

[23] Z. Wang *et al.*, "Economic and heating efficiency analysis of double-shell downhole electric heater for tar-rich coal in-situ conversion," *Case Stud. Therm. Eng.*, vol. 41, p. 102596, Jan. 2023, doi: 10.1016/j.csite.2022.102596.

[24] R. Kunwer, S. Pandey, and S.S. Bhurat, "Comparison of selected shell and tube heat exchangers with segmental and helical baffles," *Therm. Sci. Eng. Prog.*, vol. 20, p. 100712, Dec. 2020, doi: 10.1016/j.tSep..2020.100712.

[25] S. Lanzini, M. Mar.ro, M. Creyssels, and P. Salizzoni, "Helium plumes at moderate Reynolds number," *Phys. Rev. Fluids*, vol. 9, no. 6, p. 064501, Jun. 2024, doi: 10.1103/PhysRevFluids.9.064501.

[26] J.W. Rose, "Heat-transfer coefficients, Wilson plots and accuracy of thermal measurements," *Exp. Therm. Fluid Sci.*, vol. 28, no. 2–3, pp. 77–86, 2004.

[27] J.F. Yang, Y.S. Lin, H.B. Ke, M. Zeng, and Q.W. Wang, "Numerical investigation on combined multiple shell-pass shell-and-tube heat exchanger with continuous helical baffles," *Energy*, vol. 115, no. 5–6, pp. 1572–1579, 2016.

[28] J. Wu, J. Zhou, Y. Chen, M. Wang, C. Dong, and Y. Guo, "Experimental investigation on enhanced heat transfer of vertical condensers with trisection helical baffles," *Energy Convers. Manage.*, vol. 109, pp. 51–62, Feb. 1 2016, doi: 10.1016/j.enconman.2015.11.044.

[29] Q. Bu, Q. Li, and X. Li, "Numerical heat transfer simulation of oil shale large-size downhole heater," *Appl. Sci.*, vol. 14, no. 6, p. 2235, Mar. 2024, doi: 10.3390/app14062235.

[30] Robert, J., and Moffat, "Describing the uncertainties in experimental results," *Exp. Therm. Fluid Sci.*, 1988.

[31] Z. Du and W. Li, "The catalytic effect from alkaline elements on the tar-rich coal pyrolysis," *Catalysts*, vol. 12, no. 4, p. 376, Apr. 2022, doi: 10.3390/catal12040376.

Bull. Pol. Acad. Sci. Tech. Sci., vol. 73, no. 3, p. e153839, 2025

11